Journal of Magnetic Resonance 203 (2010) 100–107

Contents lists available at ScienceDirect

Journal of Magnetic Resonance

journal homepage: www.elsevier.com/locate/jmr

Intermolecular single-quantum coherence sequences for high-resolution NMR spectra in inhomogeneous fields

Yuqing Huang, Shuhui Cai, Xi Chen, Zhong Chen *

Department of Physics, Fujian Key Laboratory of Plasma and Magnetic Resonance, State Key Laboratory of Physical Chemistry of Solid Surface, Xiamen University, Xiamen 361005, PR China

ARTICLE INFO

Article history:
Received 3 September 2009
Revised 2 December 2009
Available online 14 December 2009

Keywords:
High-resolution
Magnetic resonance spectra
Intermolecular single-quantum coherences
Inhomogeneous fields
Efficient acquisition

ABSTRACT

A new pulse sequence based on intermolecular single-quantum coherences (iSQCs) is proposed to obtain high-resolution NMR spectroscopy in inhomogeneous magnetic fields via fast 2D acquisition. Taking the intrinsic properties of iSQCs, the sequence is time-efficient with a narrow spectral width in the indirect dimension. It can recover useful information of chemical shifts, relative peak areas, *J* coupling constants, and multiplet patterns even when the field inhomogeneity is severe enough to erase almost all spectroscopic information. Moreover, good solvent suppression efficiency can be achieved by this sequence even with imperfect radio-frequency pulse flip angles. Spatially localized iSQC spectroscopy was performed on a sample packed with pig brain tissue and cucumber to show the feasibility of the sequence in *in vivo* magnetic resonance spectroscopy (MRS). This sequence may provide a promising way for the applications on *in vivo* and *in situ* high-resolution NMR spectroscopy.

1. Introduction

High-resolution nuclear magnetic resonance (NMR) spectroscopy is a powerful tool in many fields, such as chemistry, materials science, and life science. A high-resolution NMR spectrum generally provides information of chemical shifts, *J* coupling constants, multiplet patterns and relative peak areas for structure and composition analysis. However, there are many circumstances where the magnetic field homogeneity is degraded or the testing objects are subject to intrinsic variation in magnetic susceptibility over the sample volume and among various structural components. Line broadening due to inhomogeneous field leads to severe signal overlap and loss of fine spectral features, which precludes NMR spectral analyses and often cannot be completely eliminated with conventional field shimming methods.

Besides the improvement and development of shimming technology [1–3], a number of NMR experimental techniques have been developed to obtain high-resolution NMR spectra in inhomogeneous magnetic fields. For example, Nagayama and co-workers proposed two-dimensional (2D) spin echo correlated spectroscopy (SECSY) for the study of biological macromolecules [4]. Blümich and co-workers developed a unilateral and mobile NMR sensor applicable at low magnetic field strengths [5,6]. Pines and co-workers employed total coherence transfer echoes based on intramolecular multiple-quantum coherences (MQCs) [7] and "shim pulses" [8]. Frydman and co-workers proposed some spatial encoding methods to recover chemical shift information in large inhomogeneous field [9,10]. Pelupessy and co-workers proposed a method based on coherence transfer between spins to obtain high-resolution spectra in inhomogeneous field with unknown spatiotemporal variations [11]. In addition, Cadars and co-workers employed 2D correlation spectroscopy to extract the chemical information from disordered solids [12]. These techniques can partially remove inhomogeneous line broadening, but they cannot provide resolved *J* coupling multiplet structure since the recovered spectral resolution is usually not enough. Recently, intermolecular multiple-quantum coherences (iMQCs) caused by long-range dipolar interactions among spins in different molecules have generated tremendous interests [13–20]. Since intermolecular dipolar interactions are effective within the range of 5–500 μm, far smaller than a typical sample dimension, it is intuitively attractive to apply iMQCs to NMR spectroscopy in inhomogeneous fields. The main advantage of iMQC methods lies on its ability to detect identical interactions for different spin groups in a molecule, therefore simultaneously retaining all desired spectral features. Warren and co-workers proposed some sequences based on intermolecular zero-quantum coherences (iZQCs): HOMOGENIZED (HOMOGeneity Enhancement by Intermolecular ZEro-quantum Detection) [21], composite CPMG-HOMOGENIZED [22], and ultrafast iZQC 2D spectroscopy technique [23]. Our group proposed iDQF-HOMOGENIZED [24] based on iZQCs, and IDEAL (Intermolecular Dipolar-interaction Enhanced All Lines) [25] (also referred to as

* Corresponding author. Fax: +86 592 2189426.
E-mail address: chenz@xmu.edu.cn (Z. Chen).

1090-7807/$ - see front matter © 2009 Elsevier Inc. All rights reserved.
doi:10.1016/j.jmr.2009.12.007

IDEAL-I) and IDEAL-II [26] based on intermolecular double-quantum coherences (iDQCs).

It is noticed that all the high-resolution iMQC methods reported to date are based upon either iZQCs or iDQCs. It has been reported that the apparent diffusion rates of iZQCs and iDQCs during the evolution period are larger than the conventional SQC ones, while the transverse relaxation times of iZQCs and iDQCs during the evolution period are shorter than the conventional SQC ones [27]. On the other hand, iSQCs have similar diffusion and relaxation behavior to the conventional SQCs during the evolution period [28], thus providing a different way for high-resolution NMR spectroscopy. Previous studies on iSQCs (or nonlinear echo) were all carried out in homogeneous fields [29–32]. In this paper, iSQCs were utilized to obtain high-resolution NMR spectra in inhomogeneous fields. A new pulse sequence, IDEAL-III, was designed for this purpose. Similar to the iZQC methods [21–24], the apparent J coupling constants in the resulting spectra are the same as those in conventional SQC spectra, thus the spectral peak overlapping caused by the magnification of apparent scalar coupling is avoided. Since only the chemical shift evolution of solvent is selected in the evolution period t_1, the iSQC signals obtained from the new sequence are not susceptible to the J coupling modulation. Moreover, the new sequence is highly time-efficient with narrow spectral width in the indirect dimension. It has good solvent suppression efficiency even with imperfect RF pulse flip angles, which may provide a promising way for the applications in *in vivo* magnetic resonance spectroscopy (MRS) where intense water resonance and inhomogeneous line broadening due to intrinsic macroscopic susceptibility gradients often substantially degrade the spectral quality of conventional proton MRS [33,34]. The feasibility of the IDEAL-III sequence in *in vivo* MRS was tested in combination with point-resolved spectroscopy (PRESS) localization [35].

2. Theories and methods

The IDEAL-III sequence is shown schematically in Fig. 1a. In the sequence, the first and the third RF pulses are selective for solvent, while the second RF pulse is selective for solute. In order to select the coherence transfer pathway $0 \rightarrow +1 \rightarrow +2 \rightarrow +1 \rightarrow -1$, three linear coherence selection gradients (CSGs) with an area ratio of 1:0.7:−2.4 are applied. In this way, the desired solvent–solute iSQCs are selected while both conventional SQCs and other iMQCs are filtered out. The excitation sculpting [36,37] applied before acquisition and a specially designed phase cycling scheme further improve the solvent suppression efficiency. Moreover, a PRESS-like module [35] can be integrated with the IDEAL-III sequence to obtain spatially localized iSQC spectra (Fig. 1b). Three slice-selective refocusing π RF pulses along orthogonal directions cannot only select the interesting region within a sample, but also refocus the iSQC signals, thus the non-selective π RF pulses in the IDEAL-III sequence can be omitted.

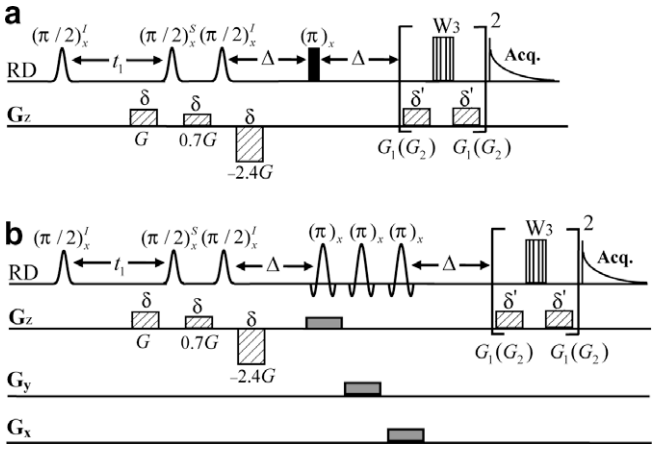

Fig. 1. Pulse sequences for high-resolution spectra in inhomogeneous fields via iSQCs: (a) IDEAL-III and (b) IDEAL-III with PRESS localization. Full vertical bar stands for non-selective RF pulses, Sinc- and Gauss-shaped pulses are selective RF pulses, dash rectangles represent coherence selection gradients, shadow rectangles represent slice-selective gradients, and vertical-line rectangle represents "W3" binomial π pulse.

In present work, without loss of generality, we consider a homogeneous liquid mixture consisting of S and I components. S is an AX spin-1/2 system (including S_k and S_l spins with scalar coupling constant J_{kl}) and I is a single spin-1/2 system. It is assumed that I (corresponding to solvent) is abundant and S (corresponding to solutes) is either abundant or dilute. Assume that ω_m is the frequency offset of spin m ($m = I, S_k, S_l$) in the rotating frame in the absence of field inhomogeneity. The background field is assumed to be only inhomogeneous along the z-axis, and $\Delta B(z)$ is the field inhomogeneity at position z. If the magnetization is fully modulated and varies only in one direction, the dipolar field is localized and an exact theoretical expression for the iMQC signal can be deduced [38]. In the following, the distant dipolar field (DDF) [39,40] treatment combined with product operator formalism is employed for theoretical deduction. For simplification, the effects of radiation damping, diffusion, relaxation, and intermolecular NOE are ignored. Since we are interested in the evolution of magnetization, we consider only a reduced density operator. For the $I + S$ spin system discussed herein, the reduced density operators σ^I_{eq} for each I proton and σ^S_{eq} for the two protons in each S molecule at initial thermal equilibrium state with the high-temperature approximation can be given by

$$\begin{aligned} \sigma^I_{eq} &= I_z, \\ \sigma^S_{eq} &= S_{kz} + S_{lz}, \end{aligned} \tag{1}$$

where the Bolzmann factor has been omitted for clarity; I_z, S_{kz}, and S_{lz} represent the longitudinal components of I, S_k, and S_l spins, respectively. Since S_k is similar to S_l in an AX spin-1/2 system, only S_k evolution is considered in the following deduction.

For the IDEAL-III sequence shown in Fig. 1a, the first selective $(\pi/2)^I_x$ RF pulse rotates I_z into $-I_y$. During the evolution period t_1, only I spin evolves under chemical shift, field inhomogeneity, and the first gradient pulse. The selective $(\pi/2)^S_x$ RF pulse rotates the S_z into transverse plane. The spin density operator then evolves under the second gradient pulse during the period δ. After the second selective $(\pi/2)^I_x$ RF pulse, the reduced density operators become

$$\begin{aligned} \sigma^I(t_1^+, z) &= -I_z \cos[\omega_I t_1 + \gamma \Delta B(z) t_1 + 1.7\gamma G \delta z] \\ &\quad + I_x \sin[\omega_I t_1 + \gamma \Delta B(z) t_1 + 1.7\gamma G \delta z], \\ \sigma^S(t_1^+, z) &= -S_{ky} \cos(0.7\gamma G \delta z) + S_{kx} \sin(0.7\gamma G \delta z), \end{aligned} \tag{2}$$

where $\gamma G \delta z$ is the dephasing angle of spins at position z due to the first CSG, in which γ is the gyromagnetic ratio, G and δ are strength and duration of the CSG, respectively; $\gamma \Delta B(z) t_1$ is the dephasing angle of spins at position z due to field inhomogeneity. Note that the density operator $\sigma^I(t_1^+, z)$ in Eq. (2) includes a spatially modulated longitudinal magnetization of I spin, which is the source DDF along the z direction. According to the DDF theory,

$$\begin{aligned} B^I_d(z) &= -\frac{\Delta_s}{\gamma \tau_d} \cos[\omega_I t_1 + \gamma \Delta B(z) t_1 + 1.7\gamma G \delta z], \\ B^S_d(z) &= \frac{2}{3} B^I_d(z) = -\frac{2\Delta_s}{3\gamma \tau_d} \cos[\omega_I t_1 + \gamma \Delta B(z) t_1 + 1.7\gamma G \delta z], \end{aligned} \tag{3}$$

where $B^I_d(z)$ and $B^S_d(z)$ represent the DDFs experienced by I and S spins at position z, respectively; $\tau^I_d = (\gamma \mu_0 M^I_0)^{-1}$ is the dipolar demagnetizing time of I spins, in which μ_0 is vacuum magnetic per-

meability and M_0^I is the equilibrium magnetization per unit volume of I spin; $\Delta_s = [3(\hat{\mathbf{s}}\cdot\hat{\mathbf{z}})^2 - 1]/2$, in which $\hat{\mathbf{s}}$ is the unit vector along the CSG direction, and $\hat{\mathbf{z}}$ is the unit vector along the direction of static magnetic field. Since the gradient field is oriented along the z direction, i.e. $\hat{\mathbf{s}} = \hat{\mathbf{z}}$, we have $\Delta_s = 1$. To avoid confusion, we used B_d^I and B_d^S to stand for $B_d^I(z)$ and $B_d^S(z)$ respectively in the following expressions.

To prevent the dephasing of signals before the DDF takes effect, a non-selective π pulse was inserted in the middle of delay interval (2Δ) to form a spin echo at the beginning of detection period. Since the module of excitation sculpting right before acquisition only acts to suppress the solvent signals and does not influence the desired solute signals, we ignore it in the following deduction. During the acquisition period t_2, the observable transverse spin densities evolve under chemical shift, field inhomogeneity, and effective dipolar field, hence,

$$\begin{aligned}\sigma^I(t_1+t_2,z) &= \{I_x\cos[-2.4\gamma G\delta z-\omega_I t_2-\gamma\Delta B(z)t_2+\gamma B_d^I(2\Delta+t_2)]\\ &\quad - I_y\sin[-2.4\gamma G\delta z-\omega_I t_2-\gamma\Delta B(z)t_2+\gamma B_d^I(2\Delta+t_2)]\}\\ &\quad\times\sin[\omega_I t_1+\gamma\Delta B(z)t_1+1.7\gamma G\delta z],\\ \sigma^S(t_1+t_2,z) &= \{S_{ky}\cos[-1.7\gamma G\delta z-\omega_{S_k}t_2-\gamma\Delta B(z)t_2+\gamma B_d^S(2\Delta+t_2)]\\ &\quad + S_{kx}\sin[-1.7\gamma G\delta z-\omega_{S_k}t_2-\gamma\Delta B(z)t_2+\gamma B_d^S(2\Delta+t_2)]\}\\ &\quad\times\cos(2\pi J_{kl}\Delta)\cos(\pi J_{kl}t_2).\end{aligned} \tag{4}$$

The total complex transverse spin magnetization at position z becomes

$$\begin{aligned}M^+(t_1+t_2,z) &= \frac{M_0^I}{2i}\left\{e^{i[\omega_I t_1+\gamma\Delta B(z)t_1+1.7\gamma G\delta z]}-e^{-i[\omega_I t_1+\gamma\Delta B(z)t_1+1.7\gamma G\delta z]}\right\}\\ &\quad\times e^{i[2.4\gamma G\delta z+\omega_I t_2+\gamma\Delta B(z)t_2]}e^{-i\gamma B_d^I(2\Delta+t_2)}\\ &\quad+\frac{iM_0^S\cos(2\pi J_{kl}\Delta)}{2}e^{i[1.7\gamma G\delta z+\omega_{S_k}t_2+\gamma\Delta B(z)t_2]}\\ &\quad\times(e^{i\pi J_{kl}t_2}+e^{-i\pi J_{kl}t_2})e^{-i\gamma B_d^S(2\Delta+t_2)},\end{aligned} \tag{5}$$

where M_0^S is the equilibrium magnetization per unit volume of S spin. Using Bessel function expansion [41], Eq. (5) can be rearranged to yield

$$\begin{aligned}M^+(t_1+t_2,z) &= \frac{M_0^I}{2i}\sum_{m=-\infty}^{\infty}i^m J_m(\xi_1)\\ &\quad\times\left\{e^{i[1.7(m+1)\gamma G\delta z+2.4\gamma G\delta z+\omega_I t_2+\gamma\Delta B(z)t_2+(m+1)\omega_I t_1+(m+1)\gamma\Delta B(z)t_1]}\right.\\ &\quad\left.-e^{i[1.7(m-1)\gamma G\delta z+2.4\gamma G\delta z+\omega_I t_2+\gamma\Delta B(z)t_2+(m+1)\omega_I t_1+(m+1)\gamma\Delta B(z)t_1]}\right\}\\ &\quad+\frac{iM_0^S\cos(2\pi J_{kl}\Delta)}{2}(e^{i\pi J_{kl}t_2}-e^{-i\pi J_{kl}t_2})\sum_{m_1=-\infty}^{\infty}i^{m_1}J_{m_1}(\xi_2)\\ &\quad\times e^{i[1.7(m_1+1)\gamma G\delta z+\omega_{S_k}t_2+m_1\omega_{S_k}t_1+\gamma\Delta B(z)t_2+m_1\gamma\Delta B(z)t_1]},\end{aligned} \tag{6}$$

where $J_m(\xi_1)$ and $J_{m_1}(\xi_2)$ are the Bessel functions with integer orders m and m_1, respectively; $\xi_1 = \gamma\mu_0 M_0^I(2\Delta+t_2)$ and $\xi_2 = \frac{2}{3}\xi_1$ are the arguments of the Bessel functions. The first term in Eq. (6) represents the detectable signals of I spin and the second term is the detectable signals of S_k spin. In order to evaluate the detectable signals from the whole sample, an average of the complex magnetization over all z positions should be taken. If the sample size is much larger than the dipolar correlation distance $d_c = \pi/(\gamma G\delta)$, the spatial averaging across the sample causes the signals to vanish unless $1.7(m\pm1) = -2.4$ for the first term and $m_1 = -1$ for the second term in Eq. (6), which are independent of the absolute position in the sample [42]. Since no integer m satisfies the equation $1.7(m\pm1) = -2.4$, the signals originated from I spin disappear during the period t_2. This indicates that the solvent signals can be eliminated through coherence selection in the IDEAL-III sequence. When $m_1 = -1$, the observable signals from S_k spin at the detection period can be given as

$$\begin{aligned}M_{S_k}^+(t_1+t_2,z) &= \frac{-M_0^S\cos(2\pi J_{kl}\Delta)}{2}J_1\left(\frac{2}{3}\gamma\mu_0 M_0^I(2\Delta+t_2)\right)\\ &\quad\times\left\{e^{i[-\omega_I t_1+(\omega_{S_k}+\pi J_{kl})t_2-\gamma\Delta B(z)t_1+\gamma\Delta B(z)t_2]}\right.\\ &\quad\left.+e^{i[-\omega_I t_1+(\omega_{S_k}-\pi J_{kl})t_2-\gamma\Delta B(z)t_1+\gamma\Delta B(z)t_2]}\right\}.\end{aligned} \tag{7}$$

Eq. (7) shows that only solvent–solute iSQC signal is selected and it splits into two peaks at $(\omega_I+\gamma\Delta B(z), \omega_{S_k}+\pi J_{kl}+\gamma\Delta B(z))$ and $(\omega_I+\gamma\Delta B(z), \omega_{S_k}-\pi J_{kl}+\gamma\Delta B(z))$ due to J coupling. If ΔB is the width of the spatially dependent field inhomogeneity along B_0 direction, the resonance frequency for the cross-peak would range between $\omega_{S_k}\pm\pi J\pm\gamma\Delta B/2$ in the F2 dimension and $\omega_I\pm\gamma\Delta B/2$ in the F1 dimension. If the spectrometer reference frequency coincides with the resonance frequency of I spin in B_0, i.e. $\omega_I = 0$, the intermolecular cross-peak between I and S spins will center at $(0,\omega_{S_k}+\pi J_{kl})$ and $(0,\omega_{S_k}-\pi J_{kl})$ and extend as separate streaks along the specific direction $\phi = \mathrm{arctg}(1) = 45^\circ$ with respect to the F1 axis. For all spins, all the streaks in the spectrum row up in the center of the F1 dimension. Although the range of the streaks are susceptible to the field inhomogeneity in both F1 and F2 dimensions, a projection of the cross-peaks to the F2 dimension results in a 1D high-resolution spectrum after the streaks are counter-clockwise rotated by 45°. Besides the influence of transverse relaxation and diffusion, the line-width of the projected spectrum mainly relies on the residual background inhomogeneous field within iSQC correlation distance. The projected spectrum has the same multiplet patterns and the same scale factor of J coupling constants as a conventional 1D SQC spectrum. The residual conventional SQC signals and the strong solvent iMQC signals are almost eliminated, and the suppression effectiveness is insensitive to the imperfection of RF pulse flip angles when a proper phase cycling scheme is applied. The analytical expression for the IDEAL-III sequence with PRESS-like localization (Fig. 1b) is similar to Eq. (7).

3. Experiments and simulations

All experiments were performed at 298 K using a Varian NMR System 500 MHz spectrometer, equipped with a 5 mm ^{1}H{^{15}N–^{31}P} XYZ indirect detection probe with three-dimensional gradient coils. A sample of histidine ($C_6H_9N_3O_2$) aqueous solution was used in an intentionally deshimmed inhomogeneous field (60 Hz linewidth) to demonstrate the capability of the new sequence. The molar ratio of $C_6H_9N_3O_2$ and H_2O was about 1:400, an extremely low concentration for solute. For the 1D conventional SQC experiments in both well-shimmed and deshimmed magnetic fields, the pulse repetition time was 5.0 s, the scan number was 64, and the acquisition time t_2 was 1.0 s. The experiments were acquired in 6.4 min. For the IDEAL-III experiments, the selective pulse for solute spins was constitutive of a $\pi/2$ hard pulse and a selective $\pi/2$ pulse with an opposite phase for solvent. The width of a $\pi/2$ hard RF pulse was extended to 45 μs by deliberately detuning the probe to suppress the effect of radiation damping during the evolution and detection periods. The width of the selective $\pi/2$ Gaussian pulse for solvent spins was 5.0 ms. The parameters for CSGs were $G = 0.1$ T/m and $\delta = 1.2$ ms. The W3 binomial π pulse [43] was used as a solvent-exclusive π pulse, while the parameters of the gradient pulses were $G_1 = 0.11$ T/m, $G_2 = 0.21$ T/m, and $\delta' = 1.0$ ms. The pulse repetition time was 4.0 s, the echo time (2Δ) was 120 ms, and the acquisition time t_2 was 0.4 s. An 8-step phase cycling was applied: the phases for the first selective RF pulse, the third selective RF pulse and the receiver were $(x,-x,x,-x,x,-x,x,-x)$, $(x,x,-x,-x,x,x,-x,-x)$, and $(x,-x,-x,x,x,-x,-x,x)$, respectively. 2950×25 points were acquired in 15 min with the spectral widths of 3500 and 100 Hz in F2 and F1

dimensions. The signals were zero filled to 8192 × 1024 before FFT. In addition, an experiment was performed with the RF pulse flip angles deviated 1/9 from the optimal values to reveal the insensitivity of the IDEAL-III sequence to the imperfection of RF pulse flip angles. That is, the width of a $\pi/2$ hard RF pulse was set as 40 μs and the width of the selective $\pi/2$ Gaussian pulse for solvent spins was 4.44 ms. Except for this difference, all the experimental parameters were kept unchanged. The sensitivity was calculated as SNR/$\sqrt{\text{acquisition time}}$ [44], where SNR is the signal-to-noise ratio calculated by dividing the intensity of the peak at 6.94 ppm by the standard deviation (SD) of noise signals in the region between 6.0 and 6.5 ppm.

A mixture of tyrosine ($C_9H_{11}NO_3$), arginine ($C_6H_{14}N_2O_4$), and water was used to demonstrate the capability of the IDEAL-III sequence for fast acquisition. The molar ratio of $C_9H_{11}NO_3$, $C_6H_{14}N_2O_4$, and H_2O was about 1:1:300. The pulse repetition time was 3.0 s and the acquisition time t_2 was 0.3 s. The magnetic field was intentionally deshimmed to produce a line-width of about 60 Hz. The spectral width was set to 100 Hz with 18 increments for the F1 dimension, and 5000 Hz for the F2 dimension. No phase cycling was used and the total experimental time was only one minute. The other parameters were the same as those for the histidine aqueous solution experiments. The spectral data were processed by sinebell window function and were zero filled to 8096 × 2048 before regular FFT.

A sample of intact pig brain tissue fitted in a 5 mm NMR tube was used to test the feasibility of the IDEAL-III sequence for samples with intrinsic macroscopic susceptibility gradients and intense water signal. All experiments were performed without locking and shimming. The probe was well tuned to preserve high sensitivity. The pulse repetition time was 3.0 s and the echo time (2Δ) was 80 ms. The CSGs with strength $G \approx 0.1$ T/m and duration $\delta = 1.2$ ms were applied. The gradient pulses for the excitation sculpting were set to $G_1 = 0.11$ T/m, $G_2 = 0.21$ T/m, and $\delta' = 1.0$ ms. The acquisition time t_2 was 0.2 s. 2000 × 12 points were acquired in 13 min with the spectral widths of 5000 and 200 Hz in the F2 and F1 dimensions. A conventional 1D experiment with excitation sculpting was performed. The parameters of this experiment were the same as those of the IDEAL-III experiment, and the scan number was 32. To confirm the results from IDEAL-III, a 1D water-presaturated spin echo experiment of pig brain tissue was also performed using a ^{1}H Nano NMR probe and a small amount of 2,2-dimethyl-2-silapentane-5-sulfonate sodium salt (DSS) was added to the sample as an internal reference standard at $\delta = 0.00$ ppm (methyl group). The sample was spun along the magic-angle (54.7°) direction at a rate of 2 kHz. For this 1D pulse sequence, a T2-edited Carr–Purcell–Meiboom–Gill (CPMG) segment with total echo time 360 ms was incorporated to selectively record the signals of small metabolites in the brain tissue. The pulse repetition time was 4.0 s and the scan number was 64.

A sample of pig brain tissue closely packed against a piece of cucumber in a 5 mm NMR tube was used to further test the feasibility of the IDEAL-III sequence on high-resolution *in vivo* MRS. The two materials were separated by a piece of plastic, with the pig brain tissue on top and the cucumber underneath. The spatially localized IDEAL-III sequence (Fig. 1b) was applied. The spin echo image of the sagittal plane was acquired. For spectral study, three-dimensional localization was applied using the PRESS module for each dimension. The voxel was set to be 4 × 4 × 16 mm^3 for localizing the whole stratified sample and 4 × 4 × 7 mm^3 for exclusively selecting the pig brain tissue or the cucumber. The width of the slice-selective refocusing π pulses was 1.5 ms. The echo time (2Δ) was 28 ms. 2000 × 12 points were acquired in 24 min with the spectral widths of 5000 and 200 Hz in the F2 and F1 dimensions. The PRESS spectra of the corresponding voxels were also acquired for comparison. The variable power and optimized relaxation delays (VAPOR) module was utilized for water suppression in the PRESS experiments.

4. Discussion

Experimental results of histidine aqueous solution are shown in Fig. 2, together with the molecular structure of histidine. A conventional 1D SQC spectrum of the sample in a homogeneous magnetic field is shown in Fig. 2a. Except for intensive water signal, five different peaks from histidine can be observed. The insets display the expanded multiplets. The magnetic field was then intentionally deshimmed to produce a line-width of 60 Hz, and the resulting 1D spectrum is illustrated in Fig. 2b. Clearly, no coupling split can be observed. The 2D IDEAL-III spectrum was acquired in the same inhomogeneous field. After a counter-clockwise rotation of 45°, the accumulated projection of the 2D spectrum onto the F2 axis together with the expanded regions of interest is presented in Fig. 2c. The line-width of the projection spectrum is reduced from 60 to 4 Hz and all the information of chemical shift, *J* coupling constant, and multiple pattern are maintained. Since all the streaks are located along the center line of F_1 dimension and only occupy a narrow frequency range in the F_1 dimension, experimental time and data size can be greatly reduced. It can be seen that the IDEAL-III sequence has amazing solvent suppression efficiency. A suppression efficiency of more than 10^5-fold can be achieved in the inhomogeneous field if a 16-step phase cycling is used. In addition, the experimental result with imperfect RF pulse flip angles is presented in Fig. 2d. From the projection spectrum and the expanded regions, we can see that the water suppression efficiency and the spectral resolution are almost unaffected by the great deviation of pulse flip angles. Note that the sensitivity of the IDEAL-III projection spectrum is only about 13.6% of that of the conventional 1D SQC spectrum in the same inhomogeneous field due to the intrinsic low SNR of iMQCs (see Fig. 2b and c).

To test the capability of the IDEAL-III sequence for fast acquisition, a sample of a mixture of tyrosine and arginine in water was placed in an inhomogeneous field with 60 Hz line-width (Fig. 3b). The molecular structures of tyrosine and arginine are given on the top right of Fig. 3. A 1D ^{1}H NMR spectrum in a well-shimmed field as well as expanded multiplets from inequivalent protons of the mixture is shown in Fig. 3a. The 2D IDEAL-III spectrum acquired in the inhomogeneous field with only one minute is displayed in Fig. 3c. The corresponding projection spectrum also achieves high solvent suppression efficiency and keeps all the solute iSQC signals. All the multiplets from the inequivalent protons are expanded and shown in Fig. 3d. Although the spectral resolution is not as good as conventional 1D spectrum and some signals are distorted, the basic information of chemical shifts, scalar coupling constants, and multiplet patterns is retained in such a short experimental time. Since the IDEAL-III spectral width in the F1 dimension only needs to cover the range of field inhomogeneity when the spectrometer reference frequency coincides with the resonant frequency of the solvent spin, the time saving can be substantial when the sample has wide chemical shift distribution.

Experiments on a sample of *in vitro* pig brain tissue fitted in a 5 mm NMR tube were carried out to test the feasibility of the IDEAL-III sequence for samples with intrinsic field homogeneity. The line-width of the water resonance (near 4.8 ppm) is about 100 Hz in the conventional 1D ^{1}H NMR spectrum (Fig. 4a). Hardly any spectral information can be obtained from this spectrum due to the intense water signal and line broadening caused by magnetic susceptibility gradients among various structural components. The conventional 1D spectrum obtained utilizing the excitation sculpting scheme for solvent suppression is shown in Fig. 4b. The resolution is still very poor. The 2D IDEAL-III spectrum after a counter-clockwise rotation of 45° and its accumulated pro-

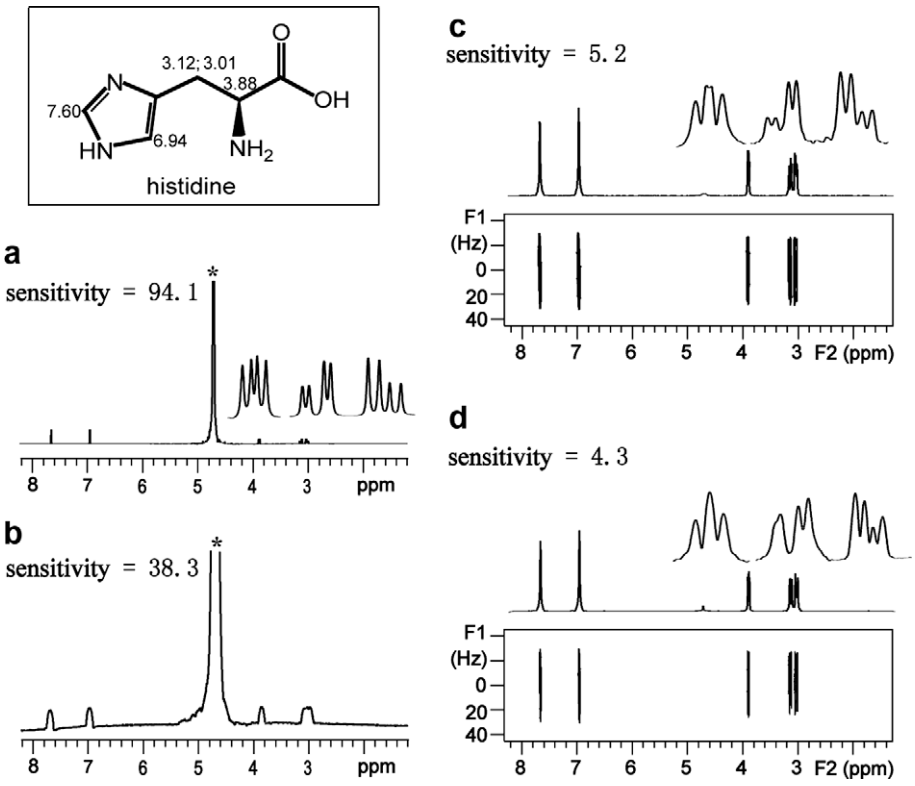

Fig. 2. ^{1}H NMR spectra of a solution of histidine in water (molar ratio is about 1:400): (a) conventional 1D high-resolution spectrum acquired in a well-shimmed field; (b) conventional 1D spectrum acquired in an inhomogeneous field with a line-width of about 60 Hz; (c) 2D IDEAL-III spectrum in the same inhomogeneous field after a counter-clockwise rotation of 45° and its accumulated projection along the F2 axis; and (d) 2D IDEAL-III spectrum obtained with the RF pulse flip angles deviated 1/9 from the optimal values and its accumulated projection along the F2 axis after a counter-clockwise rotation of 45°. The peaks marked by $*$ are truncated due to their strong intensities. The insets display the expanded multiplets. The structure of histidine is shown in the frame on the top left, together with the values of proton chemical shifts.

jection along the F2 axis are shown in Fig. 4c. It can be seen that the water signal is suppressed effectively and the weak metabolite signals are observable. The line-widths are greatly reduced and several multiplet patterns of metabolites such as lactate (Lac, 1.31 ppm), alanine (Ala, 1.47 ppm) can be resolved. However, the residual line-width in the projection spectrum is still about 13 Hz due to the intrinsic short relaxation times of the metabolites, which may hinder the resolution of some peaks. For comparison, a 1D water-presaturated spin echo spectrum of the pig brain tissue was also acquired using a Nano probe and the metabolites in the tissue were assigned according to the literature [45], as shown in Fig. 4d. A Nano probe is specifically designed for narrow-line high-resolution magic-angle spinning (MAS) spectra. The line-width in Fig. 4d is 3.5 Hz in phased mode and most multiplet patterns of the metabolites can be resolved. Except for the peaks at 1.75 and 2.90 ppm from DSS [45], the main metabolites detected in the Nano spectrum can be observed in the projection of the IDEAL-III spectrum. Compared to the (Nano) MAS technique, the IDEAL-III sequence may be more feasible and promising for the application in *in vivo* and *in situ* NMR since many *in vivo* and *in situ* samples cannot be spun.

Measurements with PRESS localization on the stratified sample of pig brain tissue and cucumber was performed to exam the feasibility of the IDEAL-III sequence in *in vivo* MRS. The spatially localized IDEAL-III sequence (see Fig. 1b) was applied. The 1D localized IDEAL-III projection spectra, normal PRESS spectra, and spin echo image of the sample are shown in Fig. 5. The 1D non-localized IDEAL-III projection spectrum from the cucumber is also presented for comparison (see Fig. 4c for the projection spectrum of the pig brain tissue). No any information can be obtained from the conventional 1D SQC spectrum with a line-width of 80 Hz and intense water signal (Fig. 5a). The sagittal spin echo image is illustrated on the top right of Fig. 5. The localized regions of the pig brain tissue and the cucumber are marked by I and II, respectively. The voxels in the pig brain tissue and the cucumber were both set to be $4 \times 4 \times 7$ mm^3. The voxel of $4 \times 4 \times 16$ mm^3 was used to localize the whole stratified sample including regions I and II. After the rotation, the projection spectrum from the IDEAL-III sequence with the whole sample localization is shown in Fig. 5b. The spectra localized in regions I and II are presented in Fig. 5c and d, respectively. It can be seen that the line-width was greatly reduced and the water signal was effectively suppressed. Compared to the spectrum in Fig. 4c, the main metabolites in the pig brain tissue can be observed in Fig. 5c. Similarly, the components detected in the 1D IDEAL-III projection spectrum of the cucumber (Fig. 5e) can also be observed in the projection of localized spectrum (Fig. 5d). Compared to the normal PRESS spectra localizing the corresponding voxels (Fig. 5f–h), the iSQC MRS from the IDEAL-III sequence can provide fine spectral information.

5. Conclusion

In this work, a new pulse sequence, IDEAL-III, was devised based on iSQCs to obtain 1D high-resolution NMR spectra in inhomogeneous fields via fast 2D acquisition. The new sequence allows efficient acquisition of high-resolution spectra in inhomogeneous fields with J coupling constants retained as in conventional SQC spectra. The DDF treatment combined with reduced density operator formalism was applied to derive analytical expression of the iSQC signals from the new sequence. The experiments were carried out in inhomogeneous fields intentionally deshimmed or arising from intrinsic macroscopic susceptibility gradients to verify the

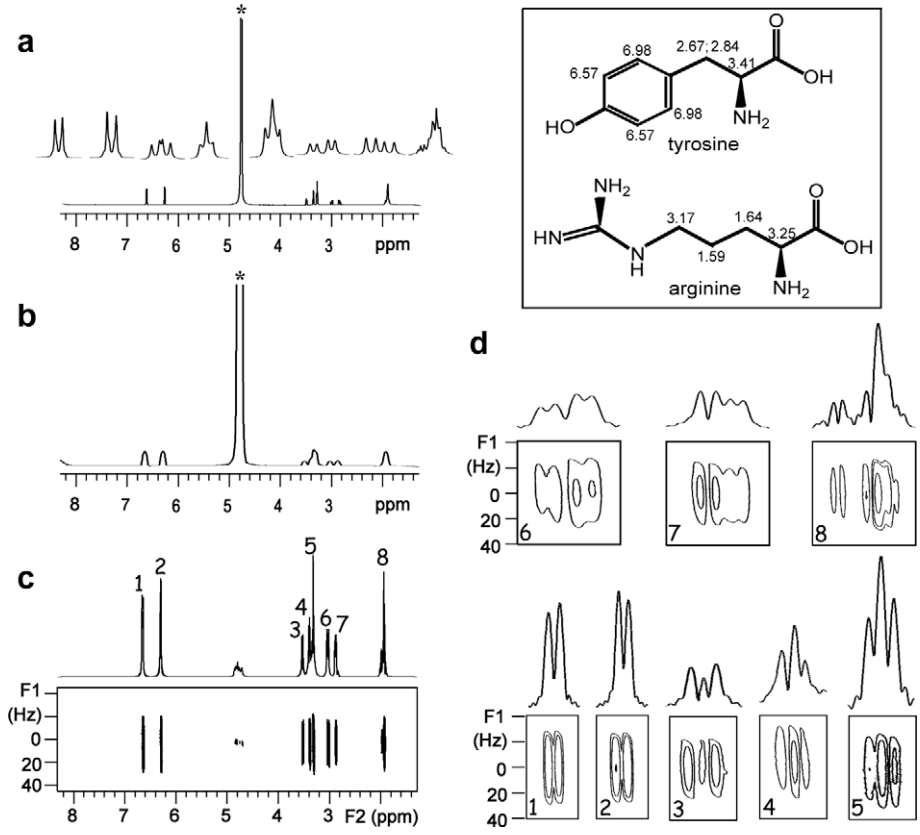

Fig. 3. ^{1}H NMR spectra of tyrosine and arginine in water (molar ratio is about 1:1:300): (a) conventional 1D high-resolution spectrum acquired in a well-shimmed field; (b) conventional 1D spectrum acquired in an inhomogeneous field with a line-width of about 60 Hz; (c) 2D IDEAL-III spectrum acquired under the same inhomogeneous field in one minute after a counter-clockwise rotation of 45° and its accumulated projection along the F2 axis; and (d) the expanded regions of the multiplets. The peaks marked by * are truncated due to their strong intensities. The structures of tyrosine and arginine are shown in the frame on the top right, together with the values of proton chemical shifts.

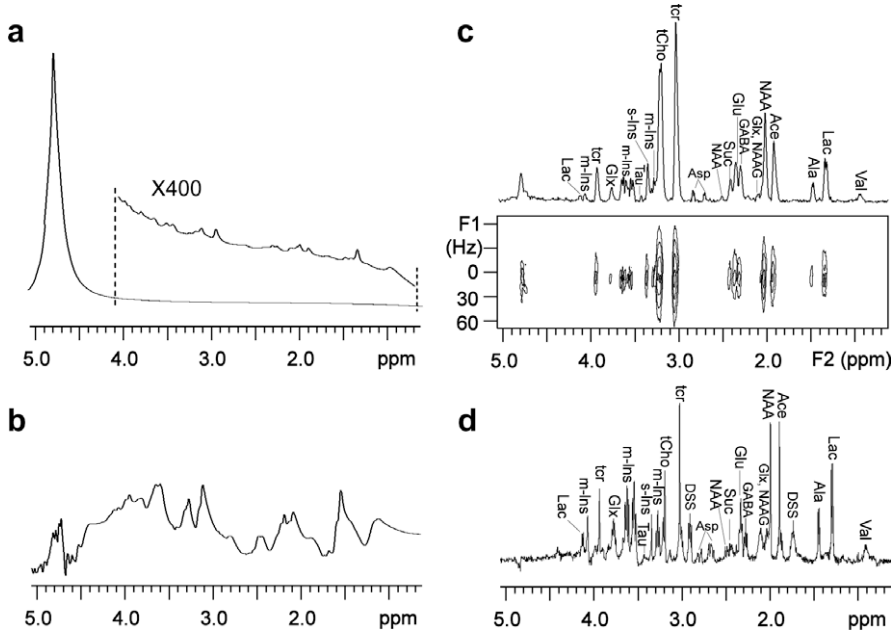

Fig. 4. ^{1}H NMR spectra of the pig brain tissue: (a) conventional 1D SQC spectrum; (b) 1D spectrum acquired with the excitation sculpting scheme; (c) 2D IDEAL-III spectrum after a counter-clockwise rotation of 45° and its accumulated projection along the F2 axis; and (d) 1D water-presaturated MAS spin echo spectrum acquired with a Nano probe.

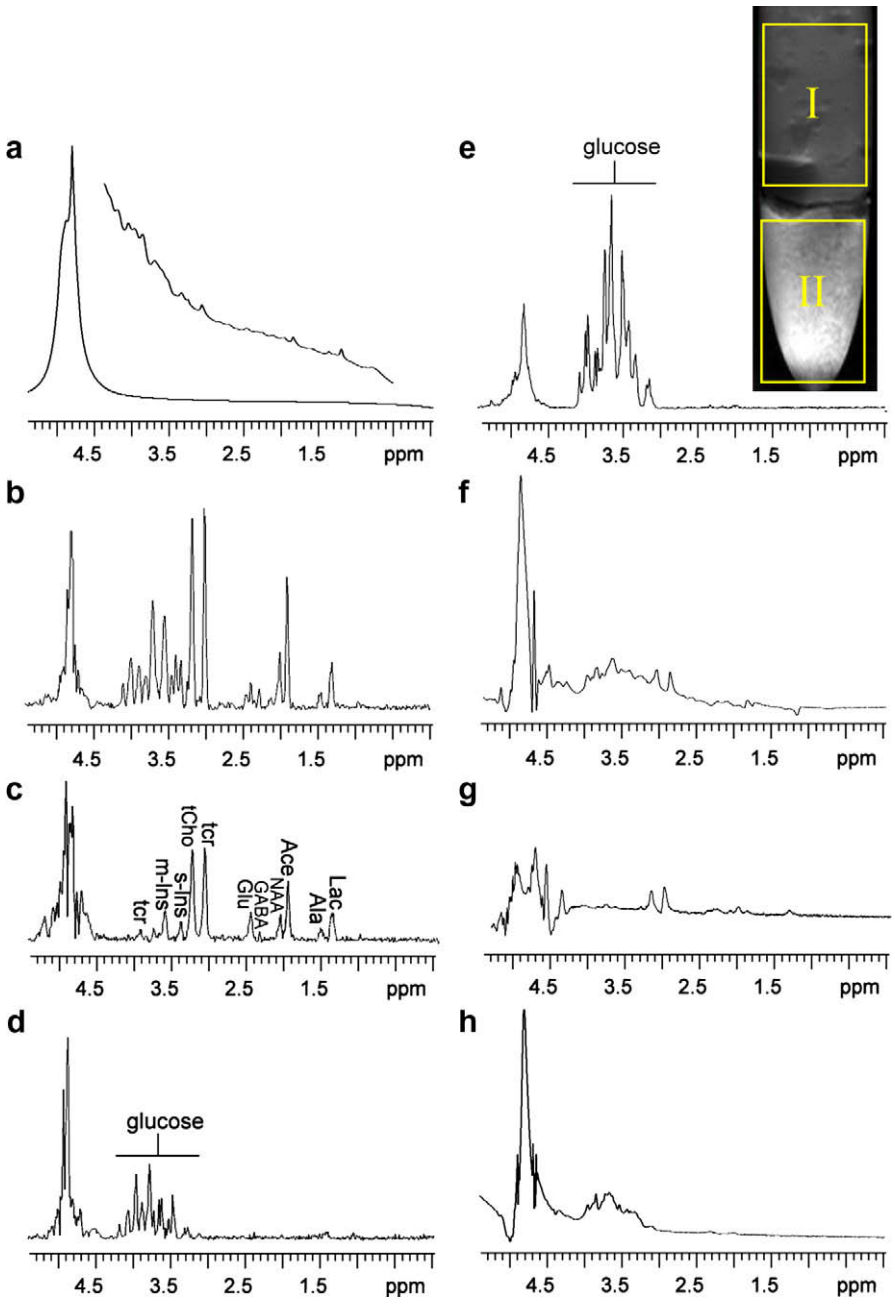

Fig. 5. ^{1}H MRS of a sample packed with pig brain tissue and cucumber: (a) conventional SQC spectrum; (b) IDEAL-III projection spectrum localizing at the whole sample; (c) IDEAL-III projection spectrum localizing at the pig brain tissue; (d) IDEAL-III projection spectrum localizing at the cucumber; (e) IDEAL-III projection spectrum of a cucumber sample; (f–h) PRESS spectra corresponding to (b–d), respectively. Spin echo image of the sample is shown on the top right and the localized regions of the pig brain tissue and cucumber are marked by I and II, respectively.

theoretical predictions and the practical feasibility of the new sequence. The results show that the theoretical predictions are in agreement with the experimental results, and this sequence may be useful for *in vivo* and *in situ* high-resolution NMR spectra. Moreover, the MRS application of the IDEAL-III sequence combined with PRESS localization on biological sample shows that high-quality iSQC localized spectra can be obtained.

The IDEAL-III sequence provides an alternative way for high-resolution NMR spectroscopy via iMQCs. Compared to the high-resolution iZQC and iDQC approaches, the new sequence is less sensitive to diffusion and relaxation losses due to the more favorable diffusion and relaxation behaviors of iSQCs during the evolution time. In general, like other iMQC high-resolution methods, the IDEAL-III sequence is applicable in small to moderate inhomogeneous fields. Since solvent-selective RF pulse is used, the maximum allowed field inhomogeneity is related to the difference between chemical shifts of solvent and its nearest solute peaks. When the field inhomogeneity reaches a certain degree, the broadened solvent peak will overlap with the broadened neighboring solute peaks. If the excitation range of the selective pulse cannot be properly set to excite only the solvent spins, the spectral quality will decrease due to the appearance of undesirable intermolecular cross-peaks arising from the distant dipolar field of solute spins, and a high-resolution spectrum may not be achievable [46]. In addition, the SNR of the iSQC signals from the new sequence is still much lower than that of conventional SQC signals. The enhancement of the spectral resolution under the inhomogeneous fields is at the cost of the SNR. Improvement of the pulse sequence for practical

applications may be achieved by combination with the dynamic nuclear polarization (DNP) technique [47,48].

Acknowledgments

This work was partially supported by the NNSF of China under Grants 10774125 and 10875101, the Key Project of Chinese Ministry of Education (109092), and National Key Technology R&D Program of China (2006BAK03A22).

References

[1] K.M. Koch, L.I. Sacolick, T.W. Nixon, S. McIntyre, D.L. Rothman, R.A. de Graaf, Dynamically shimmed multivoxel ^{1}H magnetic resonance spectroscopy and multislice magnetic resonance spectroscopic imaging of the human brain, Magn. Reson. Med. 57 (2007) 587–591.
[2] K.M. Koch, S. McIntyre, T.W. Nixon, D.L. Rothman, R.A. de Graaf, Dynamic shim updating on the human brain, J. Magn. Reson. 180 (2006) 286–296.
[3] K.M. Koch, P.B. Brown, D.L. Rothman, R.A. de Graaf, Sample-specific diamagnetic and paramagnetic passive shimming, J. Magn. Reson. 182 (2006) 66–74.
[4] K. Nagayama, K. Wuthrich, R.R. Ernst, Two-dimensional spin echo correlated spectroscopy (SECSY) for ^{1}H NMR studies of biological macromolecules, Biochem. Biophys. Res. Comm. 90 (1979) 305–311.
[5] J. Perlo, F. Casanova, B. Blümich, Single-sided sensor for high-resolution NMR spectroscopy, J. Magn. Reson. 180 (2006) 274–279.
[6] J. Perlo, V. Demas, F. Casanova, C.A. Meriles, J. Reimer, A. Pines, B. Blümich, High-resolution NMR spectroscopy with a portable single-sided sensor, Science 308 (2005) 1279.
[7] D.P. Weitekamp, J.R. Garbow, J.B. Murdoch, A. Pines, High-resolution NMR spectra in inhomogeneous magnetic fields: application of total spin coherence transfer echoes, J. Am. Chem. Soc. 103 (1981) 3578–3579.
[8] D. Topgaard, R.W. Martin, D. Sakellariou, C.A. Meriles, A. Pines, Three-dimensional phase-encoded chemical shift MRI in the presence of inhomogeneous fields, Proc. Natl. Acad. Sci. USA 101 (2004) 17576–17579.
[9] B. Shapira, L. Frydman, Spatial encoding and the acquisition of high-resolution NMR spectra in inhomogeneous magnetic fields, J. Am. Chem. Soc. 126 (2004) 7184–7185.
[10] B. Shapira, L. Frydman, Spatial encoding and the single-scan acquisition of high definition MR images in inhomogeneous fields, J. Magn. Reson. 182 (2006) 12–21.
[11] P. Pelupessy, E. Rennella, G. Bodenhausen, High-resolution NMR in magnetic fields with unknown spatiotemporal variations, Science 324 (2009) 1693–1697.
[12] S. Cadars, A. Lesage, L. Emsley, Chemical shift correlations in disordered solids, J. Am. Chem. Soc. 127 (2005) 4466–4476.
[13] W.S. Warren, W. Richter, A.H. Andreotti, B.T. Farmer, Generation of impossible cross-peaks between bulk water and biomolecules in solution NMR, Science 262 (1993) 2005–2009.
[14] A. Jerschow, Multiple echoes initiated by a single radio frequency pulse in NMR, Chem. Phys. Lett. 296 (1998) 466–470.
[15] Y.Y. Lin, N. Lisitza, S.D. Ahn, W.S. Warren, Resurrection of crushed magnetization and chaotic dynamics in solution NMR spectroscopy, Science 290 (2000) 118–121.
[16] S. Capuani, F. Curzi, F.M. Alessandri, B. Maraviglia, A. Bifone, Characterization of trabecular bone by dipolar demagnetizing field MRI, Magn. Reson. Med. 46 (2001) 683–689.
[17] S. Capuani, R.T. Branca, M. Alesiani, B. Maraviglia, Intermolecular double-quantum NMR techniques to probe microstructures on porous media, Magn. Reson. Imaging 21 (2001) 413–414.
[18] P.L. de Sousa, D. Gounot, D. Grucker, Flow effects in long-range dipolar field MRI, J. Magn. Reson. 162 (2003) 356–363.
[19] P.L. de Sousa, D. Gounot, D. Grucker, Observation of diffraction-like effects in Multiple Spin Echoe (MSE) experiments in structured samples, C. R. Chim. 7 (2004) 311–319.
[20] W. Ling, U. Eliav, G. Navon, A. Jerschow, Chemical exchange saturation transfer by intermolecular double-quantum coherences, J. Magn. Reson. 194 (2008) 29–32.
[21] S. Vathyam, S. Lee, W.S. Warren, Homogeneous NMR spectra in inhomogeneous fields, Science 272 (1996) 92–96.
[22] Y.Y. Lin, S. Ahn, N. Murali, W. Brey, C.R. Bowers, W.S. Warren, High-resolution >1 GHz NMR in unstable magnetic fields, Phys. Rev. Lett. 85 (2000) 3732–3735.
[23] G. Galiana, R.T. Branca, W.S. Warren, Ultrafast intermolecular zero quantum spectroscopy, J. Am. Chem. Soc. 127 (2005) 17574–17575.
[24] X. Chen, M.J. Lin, Z. Chen, S.H. Cai, J.H. Zhong, High-resolution intermolecular zero-quantum coherence spectroscopy under inhomogeneous fields with effective solvent suppression, Phys. Chem. Chem. Phys. 9 (2007) 6231–6240.
[25] Z. Chen, Z.W. Chen, J.H. Zhong, High-resolution NMR spectra in inhomogeneous fields via IDEAL (Intermolecular Dipolar-interaction Enhanced All Lines) method, J. Am. Chem. Soc. 126 (2004) 446–447.
[26] Z. Chen, S.H. Cai, Z.W. Chen, J.H. Zhong, Fast acquisition of high-resolution NMR spectra in inhomogeneous fields via intermolecular double-quantum coherences, J. Chem. Phys. 130 (2009) 084504.
[27] Z. Chen, Z.W. Chen, J.H. Zhong, Quantitative characterization of intermolecular dipolar interactions of two-component systems in solution nuclear magnetic resonance, J. Chem. Phys. 115 (2001) 10769–10779.
[28] Z. Chen, Z.W. Chen, J.H. Zhong, Observation and characterization of intermolecular homonuclear single-quantum coherences in liquid nuclear magnetic resonance, J. Chem. Phys. 117 (2002) 8426–8435.
[29] R. Bowtell, Indirect detection via the dipolar demagnetizing field, J. Magn. Reson. 100 (1992) 1–17.
[30] I. Ardelean, E. Kossel, R. Kimmich, Attenuation of homo- and heteronuclear multiple spin echoes by diffusion, J. Chem. Phys. 114 (2001) 8520–8529.
[31] E. Kossel, R. Kimmich, I. Ardelean, The influence of J-coupling on heteronuclear nonlinear (or multiple) spin echoes, Chem. Phys. Lett. 347 (2001) 157–162.
[32] W.R. Warren, S.Y. Huang, S. Ahn, Y.Y. Lin, Understanding third-order dipolar effects in solution nuclear magnetic resonance: Hahn echo decays and intermolecular triple-quantum coherences, J. Chem. Phys. 116 (2002) 2075–2084.
[33] D.Z. Balla, G. Melkus, C. Faber, Spatially localized intermolecular zero-quantum coherence spectroscopy for *in vivo* applications, Magn. Reson. Med. 56 (2006) 745–753.
[34] R.A. Wind, J.Z. Hu, *In vivo* and *ex vivo* high-resolution ^{1}H NMR in biological systems using low-speed magic angle spinning, Prog. Nucl. Magn. Reson. Spectr. 49 (2006) 207–259.
[35] J. Felblinger, B. Jung, J. Slotboom, C. Boesch, R. Kreis, Methods and reproducibility of cardiac/respiratory double-triggered ^{1}H-MR spectroscopy of the human heart, Magn. Reson. Med. 42 (1999) 903–910.
[36] T.L. Hwang, A.J. Shaka, Water suppression that works. Excitation sculpting using arbitrary wave-forms and fulsed-field gradients, J. Magn. Reson. 112 (1995) 275–279.
[37] A. Jerschow, Unwanted signal Leakage in excitation sculpting with single axis gradients, J. Magn. Reson. 137 (1999) 206–214.
[38] T. Enss, S. Ahn, W.S. Warren, Visualizing the dipolar field in solution NMR and MR imaging: three-dimensional structure simulations, Chem. Phys. Lett. 305 (1999) 101–108.
[39] R. Bowtell, R.M. Bowley, P. Glover, Multiple echoes in a liquid in a high magnetic field, J. Magn. Reson. 88 (1990) 643–651.
[40] J. Jeener, A. Vlassenbroek, P. Broekaert, Unified derivation of the dipolar field and relaxation terms in the Bloch-Redfield equations of liquid NMR, J. Chem. Phys. 103 (1995) 1309–1332.
[41] P.M. Morse, H. Feshbath, Methods of Theoretical Physics, McGraw-Hill, New York, 1953.
[42] S. Lee, W. Richter, S. Vathyam, W.S. Warren, Quantum treatment of the effects of dipole–dipole interactions in liquid nuclear magnetic resonance, J. Chem. Phys. 105 (1996) 874–900.
[43] V. Sklenar, M. Piotto, R. Leppik, V. Saudek, Gradient-tailored water suppression for 1H–15N HSQC experiments optimized to retain full sensitivity, J. Magn. Reson. 102 (1993) 241–245.
[44] R.R. Ernst, G. Bodenhausen, A. Wokaun, Principles of Nuclear Magnetic Resonance in One and Two Dimensions, Clarendon Press, Oxford, 1987.
[45] V. Govindaraju, K. Young, A.A. Maudsley, Proton NMR chemical shifts and coupling constants for brain metabolites, NMR Biomed. 13 (2000) 129–153.
[46] W. Zhang, C.B. Cai, S.H. Cai, X. Chen, Z. Chen, Intermolecular double-quantum coherence NMR spectroscopy in moderate inhomogeneous fields, Spectrochim. Acta A 74 (2009) 1138–1144.
[47] E.R. Jenista, R.T. Branca, W.S. Warren, Hyperpolarized carbon-carbon intermolecular multiple quantum coherences, J. Magn. Reson. 196 (2009) 74–77.
[48] M. Mishkovsky, U. Eliav, G. Navon, L. Frydman, Nearly 10^6-fold enhancements in intermolecular ^{1}H double-quantum NMR experiments by nuclear hyperpolarization, J. Magn. Reson. 200 (2009) 142–146.